Fermi National Accelerator Laboratory

FERMILAB-Conf-90/42 -E
[E-741/CDF]

Search for the Top Quark in Electron-Muon Events with CDF*

The CDF Collaboration

presented by

Angela Barbaro-Galtieri
Lawrence Berkeley Laboratory
Berkeley, California 94720

February 9, 1990

* Invited talk presented at the 8th Topical Workshop on $p\bar{p}$ Collider Physics, Castiglione della Pescaia, Italy, September 1-5, 1989.

Operated by Universities Research Association Inc. under contract with the United States Department of Energy

CDF/DOC/HEAVYFLAVOR/PUBLIC/1134
Conf-90/42-E
[E-741/CDF]

Search for the Top Quark in Electron-Muon Events with CDF

The CDF Collaboration †

Presented by Angela Barbaro-Galtieri*
Lawrence Berkeley Laboratory, University of California
Invited talk at the 8th Workshop on Proton-Antiproton Collider Physics
Castiglione della Pescaia, Italy, September 1-5 , 1989

Abstract

The CDF detector has collected data for an integrated luminosity of 4.4 pb^{-1} during the 1988-89 Tevatron Collider run. This sample has been used to search for the top quark. We report here the results of the analysis of the electron-muon topology. We find that a top mass in the 28 to 72 GeV is excluded at the 95% confidence level. The same limits apply to a possible fourth generation, charge -1/3, b' quark decaying via the charged current.

1 INTRODUCTION

The Standard Model includes three lepton and three quark doublets. While the u,d,s, quarks were discovered a posteriori, i.e., after many of their states had been discovered individually, the charm[1] and bottom[2] quarks have appeared unexpectedly with large signals in a cross section[1] or an invariant mass plot[2]. The sixth quark, the top, has been sought actively ever since the bottom quark was discovered in 1977.

Present experimental limits come from e^+e^- machines, TRISTAN, $M_{top} > 29$ GeV[3] and from the CERN Hadron Collider, UA1, $M_{top} > 41$ GeV[4].

Fits to standard model parameters using the Kobayashi-Maskawa-Cabibbo matrix and information from $B - \bar{B}$ mixing provide a limit of $M_{top} > 50$ GeV[5]. Radiative corrections to the W and Z mass provide an upper limit of $M_{top} = 180$–200 GeV[6]. So, the range

†CDF is a collaboration of the following Institutions:Argonne National Laboratory; Brandeis University; University of Chicago; Fermi National Laboratory; INFN, Laboratory Nazionali di Frascati; Harvard University; University of Illinois; KEK, Japan; Lawrence Berkeley Laboratory; University of Pennsylvania; INFN,University and Scuola Normale Superiore of Pisa; Purdue University; Rockefeller University; Rutgers University; Texas A&M University; University of Tsukuba, Japan; Tufts University; University of Wisconsin

*This work was supported in part by the Director, Office of Energy Research, Office of High Energy and Nuclear Physics, Division of High Energy Physics of the U.S. Department of Energy under Contract DE-AC0376SF00098.

of possible masses for the top quark is rather limited, yet many phenomena within the Standard Model are strongly dependent on the top mass.

We report here the results of a search for the top quark in $p\bar{p}$ collision at 1.8 TeV at the Tevatron collider. The data consists of 4.4 pb^{-1} collected in the CDF detector[7] in the 1988-1989 collider run.

Top production at a hadron collider can take place, in the lowest order, through the electroweak process $p\bar{p} \rightarrow W \rightarrow t + \bar{b}$ or the hard scattering process $p\bar{p} \rightarrow t\bar{t}$. For the first process to occur the top mass has to be below the W mass. Figure 1 shows the total cross sections for the two processes[8] at $\sqrt{s} = 0.63$ and 1.8 TeV. Note that at the Tevatron Collider top production through the electroweak process is always lower than that from hard scattering, therefore it is not considered in this analysis. The hard scattering cross sections of Fig. 1, are obtained by combining the higher order calculations of Nason et al[9], with the structure functions of Diemoz et al.[10], using the method of Altarelli et al.[11] Uncertainties due to choice of Q^2 scale and Λ_{QCD} are shown by the bands.

The decay of the top via the weak charged current into a bottom quark and a virtual (real for $M_{top} > m_W + m_b$) W , provides the signatures to be exploited for a top search. In the naive parton model the relative rates for the different top decay modes are

$t + \bar{t} \rightarrow b\bar{b}$	+	4 jets	(44.2%)	
$\rightarrow b\bar{b}$	+	2 jets + $\ell + \nu$	3(14.8%)	
$\rightarrow b\bar{b}$	+	$\ell_1\nu_1 + \ell_2\nu_2$	3(2.5%)	$\ell_1 \neq \ell_2$
$\rightarrow b\bar{b}$	+	$\ell_1\nu_1 + \ell_2\nu_2$	3(1.25%)	$\ell_1 = \ell_2$

The most copious channel is produced by the multijet decay mode, but it suffers from severe backgrounds, since the QCD multijet production is several orders of magnitude larger. A much cleaner signature consists of high P_T leptons in the event. The CDF collaboration will report here on the second and third of these channels, i.e., on the electron + jets topology[12] and the $e\mu$ topology.

Backgrounds to leptonic decays of top come from other physics processes and from lepton misidentification. Figure 2 shows the electron P_T spectrum obtained from top production at several masses and from the major competing processes: W production (associated with one or more jets) and $b\bar{b}$ pair production. These rates were obtained with the PAPAGENO Monte Carlo[13] and include higher order diagrams. No detector simulation is included. Figure 2 illustrates the importance of understanding the different topologies and the necessity of effective methods to reduce backgrounds. For the $e\mu$ channel the major physics background comes from $b\bar{b}$ production and from $Z^0 \rightarrow \tau\bar{\tau}$ giving an electron and a muon in the final state.

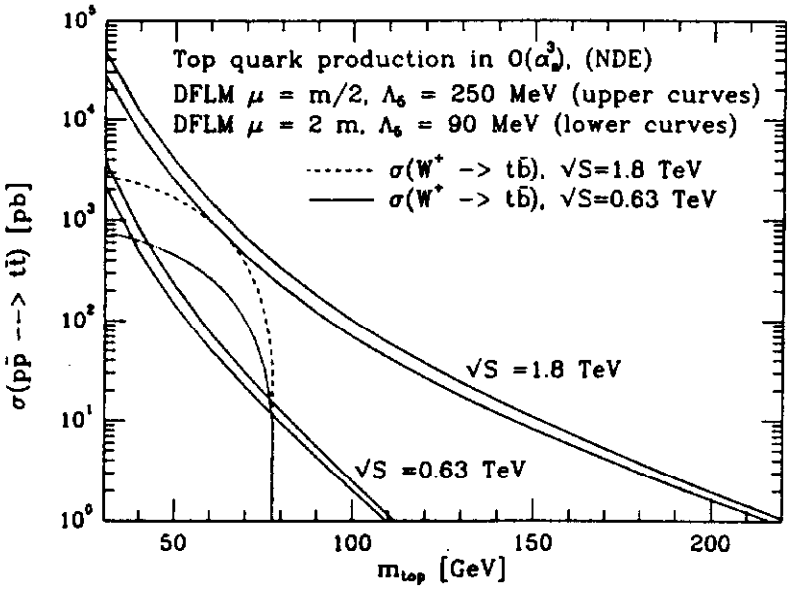

Fig. 1. Top pair production cross section versus top mass, as calculated by K. Ellis[8], using the method of Altarelli et al.[11]. The next to leading order calculations of Nason et al.[9] and the DFLM structure functions[10] are used. The bands represent the uncertainty due to μ scale and the range in Λ_5. The $W \to t\bar{b}$ cross section is also included.

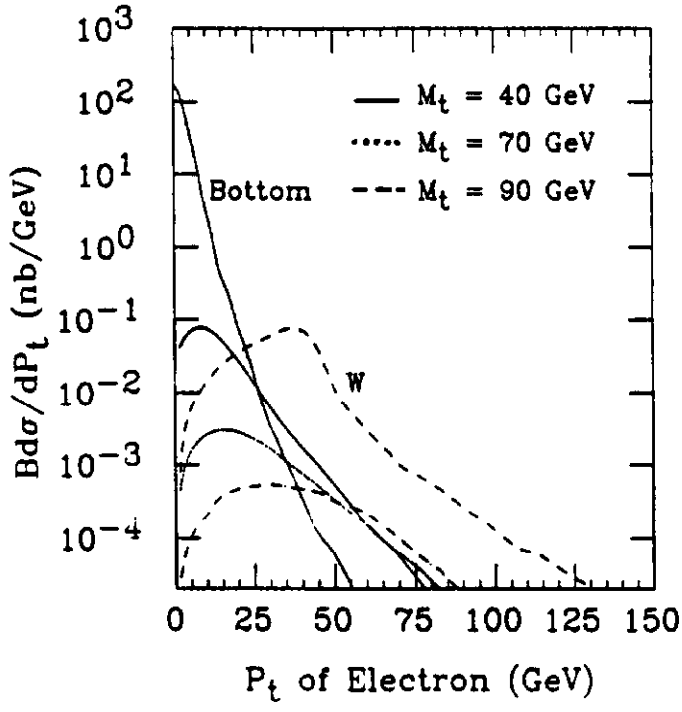

Fig. 2. Inclusive $P_\perp$ distribution of the electron from top and bottom semileptonic decays and for $W \to e\nu$, calculated using the PAPAGENO Monte Carlo. Only the branching ratio into electron has been included in the rate,i.e., no detector simulation is included.

2 THE CDF DETECTOR

The CDF detector[7] is a solenoidal detector with tracking and calorimetry covering almost the full solid angle, and with muon coverage over the central and forward region. A side view of one half of the detector is shown in Fig. 3. We describe briefly the parts relevant to this analysis; details can be found in Ref. 7.

Charged particle tracking is provided by the Vertex Time Projection Chamber (VTPC) located just outside the beam pipe from a radius of 5 cm to a radius of 22 cm and extending to a pseudorapity $\eta = 3.25$ ($\eta = -\ln(\tan(\theta/2)$, where θ is the polar angle). Outside the VTPC is a large cylindrical drift chamber (CTC) containing 60 (24) layers of axial ($\pm 3^0$ stereo angle) sense wires organized into five (four) superlayers, that extend to η =1.2 and to a radius of 1.38 m. Both tracking chambers are inside a 1.41 T solenoid which is 5 meters long. The CTC momentum resolution[14] is $\delta(P_T)/P_T = .0017 P_T$ where P_T is in GeV/c. When the vertex constraint is included the resolution is $\delta(P_T)/P_T = .0011 P_T$. In this analysis the VTPC is used for locating the event vertex with an accuracy of about 3 mm rms and to reject electron pairs from gamma conversions in the electron sample. The total amount of material between the event vertex and the CTC is 3% of a radiation length[7].

The calorimetry used in this analysis consists of the central electromagnetic (CEM), the central hadron(CHA) and the wall hadron (WHA) calorimeters. These calorimeters are segmented in a projective geometry consisting of towers of 15^0 in azimuth by 0.1 unit of rapidity. The CEM is a lead-scintillator sampling calorimeter with a single layer strip chamber (CES) with cathode and wire readout, located at shower maximum (approx. 6 radiation lengths). This chamber provides position (with a resolution of $\pm$2.5 mm at 25 GeV in the $r\phi$ direction) and lateral shape of the electromagnetic showers in the $|\eta|$ <1.1 region. The energy resolution of the CEM[14] is $15\%/\sqrt{E_T} \oplus 1.7\%$, where the 1.7% term represents the average uncertainty in the individual tower calibration. The additional systematic uncertainty on the energy scale is 0.4%. The hadron calorimeters are steel-scintillator sampling calorimeters and have a resolution of 11% at 50 GeV, as measured in a pion beam[7]. The rest of the calorimeters, plug and forward regions down to η=4.2, consist of many layers of MWPC sandwiched with lead for the EM compartment and steel for the HAD compartment. The segmentation of the gas calorimeters is of 5^0 by 0.1 units of rapidity. Finally, outside the central calorimeters, which are approximately 5 absorption length deep, are four layers of streamer chambers for muon identification in the region $|\eta|$ <0.65. As we will see later, for this analysis the muon coverage has been extended to $|\eta|$=1.2 by using CTC tracks that appear as minimum ionizing in the calorimeters.

3 ELECTRON AND MUON TRIGGERS

The CDF trigger system has two levels of hardware triggers followed by a software (Level-3) trigger that utilizes a farm of processors running offline-like algorithms. These triggers require as a prerequisite the presence of an inelastic $p\bar{p}$ collision, signalled by a coincidence between two scintillator systems, beam-beam counters, located along the beam pipe at the beginning of the forward and backward arms (Figure 3).

The trigger used for this analysis is an "inclusive electron" trigger with $P_T > 12$ GeV in the central region. We will also show some preliminary results from an "eμ" trigger for which $P_T > 5$ GeV was required for both the electron and the muon.

For the "inclusive electron" trigger, Level-1 required a CEM trigger tower ($15^0 \times$ 0.2 unit of rapidity) with an E_T of at least 6 GeV. Level-2 utilizes cluster finding and a track finder microprocessor. For each cluster with a hadronic to electromagnetic energy ratio $< .125$ and an EM cluster with $E_T > 12$ GeV, Level-2 requires a match in ϕ with a track which has a P_T of at least 6 GeV/c. Level-3 utilizes a better clustering algorithm, and geometry and strip information to further reduce the trigger rate to approximately 250 nb. Offline studies find that this trigger is (98.0$\pm$0.5)% efficient for electrons with $E_T > 15$ GeV.

For the "electron-muon" trigger, the requirements on the electron are similar to the above, with lower thresholds. For the muon the Level-1 requires a muon stub in the muon chambers. Level-2 requires a CTC track found by the fast tracker with $P_T > 5$ GeV. Finally, Level-3 uses offline two-dimensional CTC tracking and requires a track with $P_T > 5$ GeV/c matched in ϕ to the muon stub. This trigger has a rate of approximately 50 nb.

4 ELECTRON IDENTIFICATION

The identification of electrons in the region of $|\eta| < 1.0$ of the CDF detector uses information from the tracking chambers, the central calorimeters and the strip chambers (CES). The electron/pion separation has been studied in the test beam and verified with data taken at the collider[15] using an unbiased sample of electrons,i.e., the $W \rightarrow e\nu$ sample obtained by triggering on the neutrino. The offline analysis required a missing $E_T > 30$ GeV in the event, and a CEM cluster with $E_T > 30$ GeV matched to a reconstructed track; thus this "golden W" sample is expected to provide an unbiased sample of electrons.

Two of the variables used for electron identification are shown in Figure 4. Fig. 4a shows a variable that uses information from the calorimeter clusters, i. e., the intrinsic isolation cut R= (hadronic energy)/(electromagnetic energy) for the electron candidate cluster. Test beam data for electrons and pions are shown, as well as electrons from

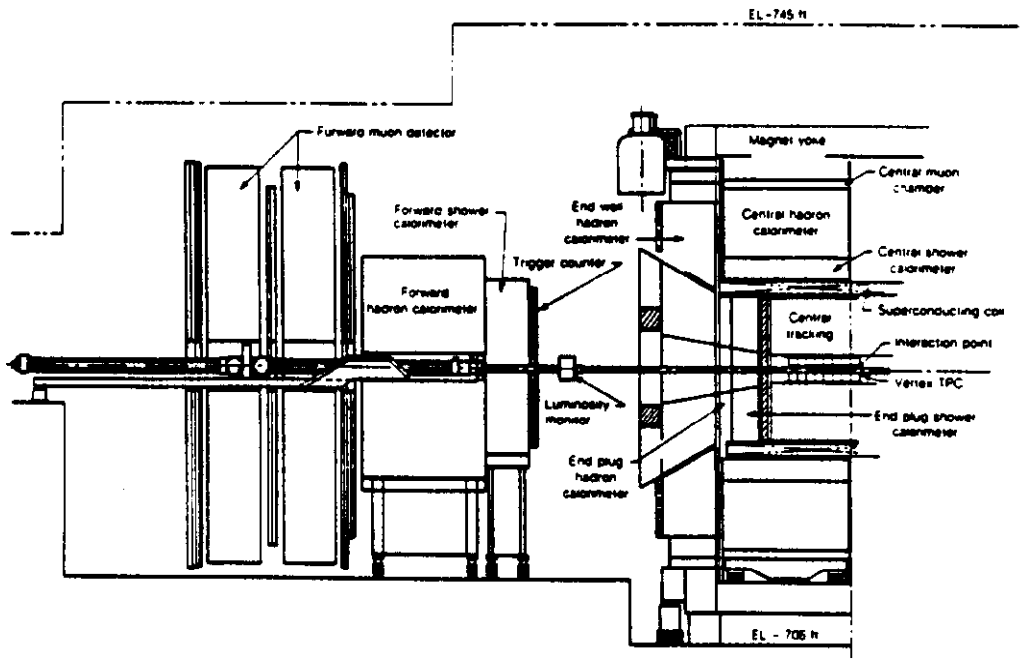

Fig. 3. Side view of the CDF Detector[7].

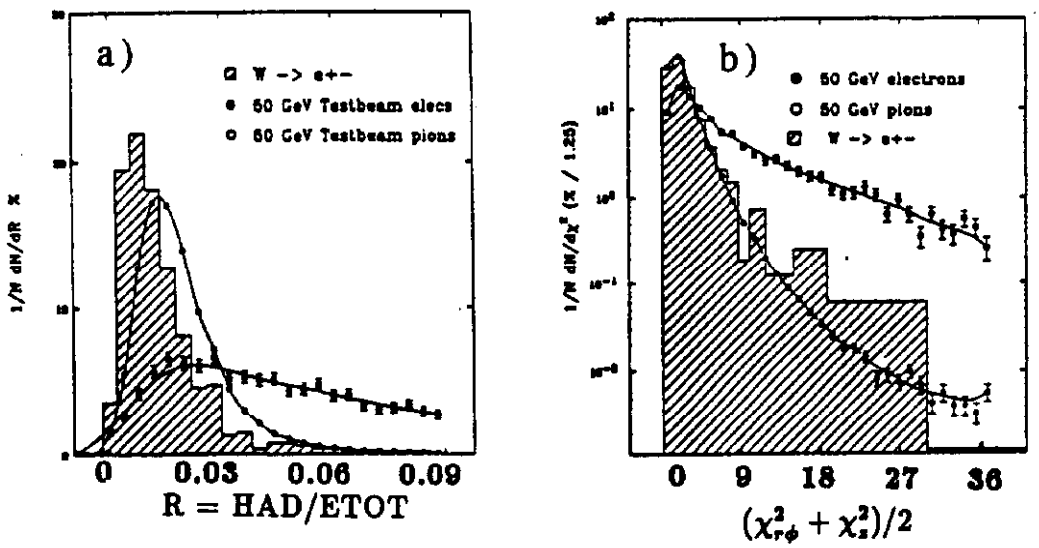

Fig. 4. Some of the variables used for electron identification[15]. Test beam data for 50 GeV electrons and pions are compared with electrons of the "golden W" sample, required to have E/P>0.9 (see text): a. hadronic energy fraction; b. the χ^2 distribution for the shower shape, measured at the proportional chambers (CES) located at shower maximum.

the "golden W" sample. A cut at R < 0.05 reduces the pion contribution considerably, preserving a good fraction of the electrons. Figure 4b shows a variable that uses the information from the CES. Here the shower shapes in both the rϕ direction, provided by the wires, and the Z direction , provided by the strips, are compared with the electron shower shapes measured in the test beam. A χ^2 is formed in each dimension, and its average is displayed in Fig. 4b. A cut at an average $\chi^2 < 10$ reduces the pion background, while keeping a good fraction of the electrons.

The other variables used for electron identification are shown in Figure 5, for the same electron sample. The LSHR variable[15] uses the calorimeter towers and requires their energy to be distributed according to test beam data: >90% of the times the electron energy is all in one tower. The rϕ and Z match again refer to CES information: the position of the shower in the strip chambers should match with the position extrapolated from the CTC measurement. Finally, the E/P ratio refers to the matching of the calorimeter energy and the electron momentum measured in the CTC. The cut at 1.5 allows for electron radiation losses in the CTC.

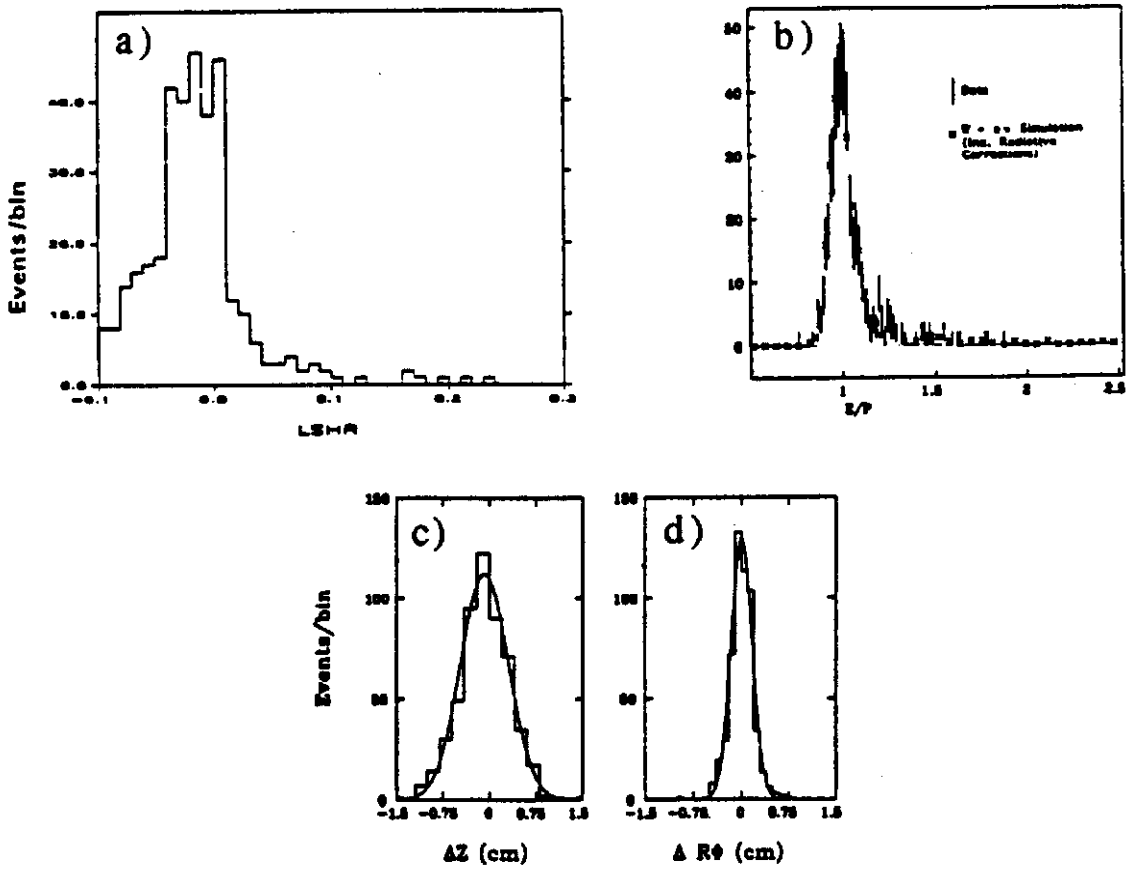

Fig. 5. Additional electron identification variables as obtained from the "golden W" sample[15]: a) the LSHR variable; b) the E/P ratio compared with a Monte Carlo simulation that includes radiation corrections; track-strip chamber match in c) the Z direction, and d) the rϕ direction.

Table I lists all the criteria used for electron identification on the data obtained with the "inclusive electron" trigger, and the efficiency of each cut. First, fiducial cuts are applied to eliminate bad regions between calorimeter modules (ϕ cracks) and region of diminished response. These cuts retain (84±2)% of the region with $|\eta| < 1$. The electron selection cuts listed in the table have a total detection efficiency of (77±3)%. The rϕ and Z match cuts shown in the table are higher than those implied by Fig. 5. This is because the CES survey parameters have not been included in the analysis of the whole sample and the distributions are wider than those of the "golden W" sample.

Table I. Selection cuts and efficiencies for electrons from $Z^0 \rightarrow e^+e^-$ with E_T >20 GeV in the $|\eta| < 1.0$ region of the calorimeter.

Cut type	Cut Value	Efficiency (%)
Fiducial		84 ± 2
Hadron/em	< 0.05	96.8 ± 1.3
LSHR	< 0.2	97.8 ± 1.1
rϕ match	< 1.5 cm	98.9 ± 0.8
Z match	< 2.0 cm	99.5 ± 0.5
Wire χ^2	< 10	86.5 ± 2.5
Strip χ^2	< 10	96.6 ± 1.7
E/P	< 1.5	92.5 ± 1.9
		77.4 ± 3.1

The efficiencies were obtained from a $Z \rightarrow e^+e^-$ sample where the first electron had the tight requirements of Table I, and the second electron had very loose requirements. This second electron is then used to find the efficiencies for each cut. The electron E_T is required to be above 20 GeV. Similar results are obtained from the W sample as described above.

After these cuts a total of 17500 events remain in the sample.

The electron sample thus obtained is contaminated with electrons from photon conversions. These are removed by requiring the presence of a VTPC track matching the CTC track and by vetoing on electrons with a nearby oppositely charged track forming a low mass e^+e^- pair. This cut also reject electrons from Dalitz decays of neutral pions. The efficiency of this algorithm is estimated to be 88%, but it also rejects approximately 5% of the good electron candidates. At this point a total of 13300 electron candidates remain, with a background of <20% , estimated from the tails of the cut variables.

5 MUON IDENTIFICATION

Muon identification uses calorimeter information as well as tracking chamber (CTC) information. As mentioned earlier, by requiring minimum ionizing signals in the calorimeters the η coverage is extended to $|\eta|$ <1.2, well beyond the muon chambers solid angle. The muon selection criteria for the separate regions (a. and b.) are shown in Table II along with the corresponding efficiencies.

First we apply fiducial cuts to avoid cracks between calorimeter modules; this keeps 85% of the total solid angle for $|\eta|$ <1.2. The CTC track for the muon candidate must have an impact parameter within 0.5 cm of the event vertex and a Z position, at point of closest approach, within 5 cm of the vertex. These requirements have a 100% efficiency. For both classes of muons the calorimeter response in the tower where the track extrapolates must have EM and HAD energy consistent with a minimum ionizing particle (see Table II). On the average a minimum ionizing particle will deposit 0.3 GeV in the EM and 2 GeV in the HAD calorimeters, as shown in Fig. 6.

Table II. Muon selection criteria and efficiencies.

Type of cut	Cut Value	Efficiency (%)
Fiducial		85.0 ± 2.0
a. For $\|\eta\|$ <.65, P_T	> 5 GeV	
EM (tower)	< 2.0 GeV	99.0 ± 1.0
HAD(tower)	< 6.0 GeV	99.0 ± 1.0
EM + HAD (towers)	> 0.1 GeV	100
rϕ matching	< 10 cm	100
		97.9 ± 1.5
b. For $\|\eta\|$ =0.65-1.2, P_T	> 10 GeV	
EM (tower)	< 2.0 GeV	100
HAD(tower)	< 6.0 GeV	95.7 ± 2.5
EM + HAD (towers)	> 0.1 GeV	100
E_T (cone δ R<.4)	< 5 GeV	100
		95.7 ± 2.5

The track P_T cut is different for the two class of muons, (5 and 10 GeV/c respectively), to reduce hadron background. For the muons of class a. an additional requirement of track-muon chamber matching within 10 cm is imposed. For muon candidates in class b. an additional calorimetry requirement is imposed, i.e., that the E_T in the towers inside a

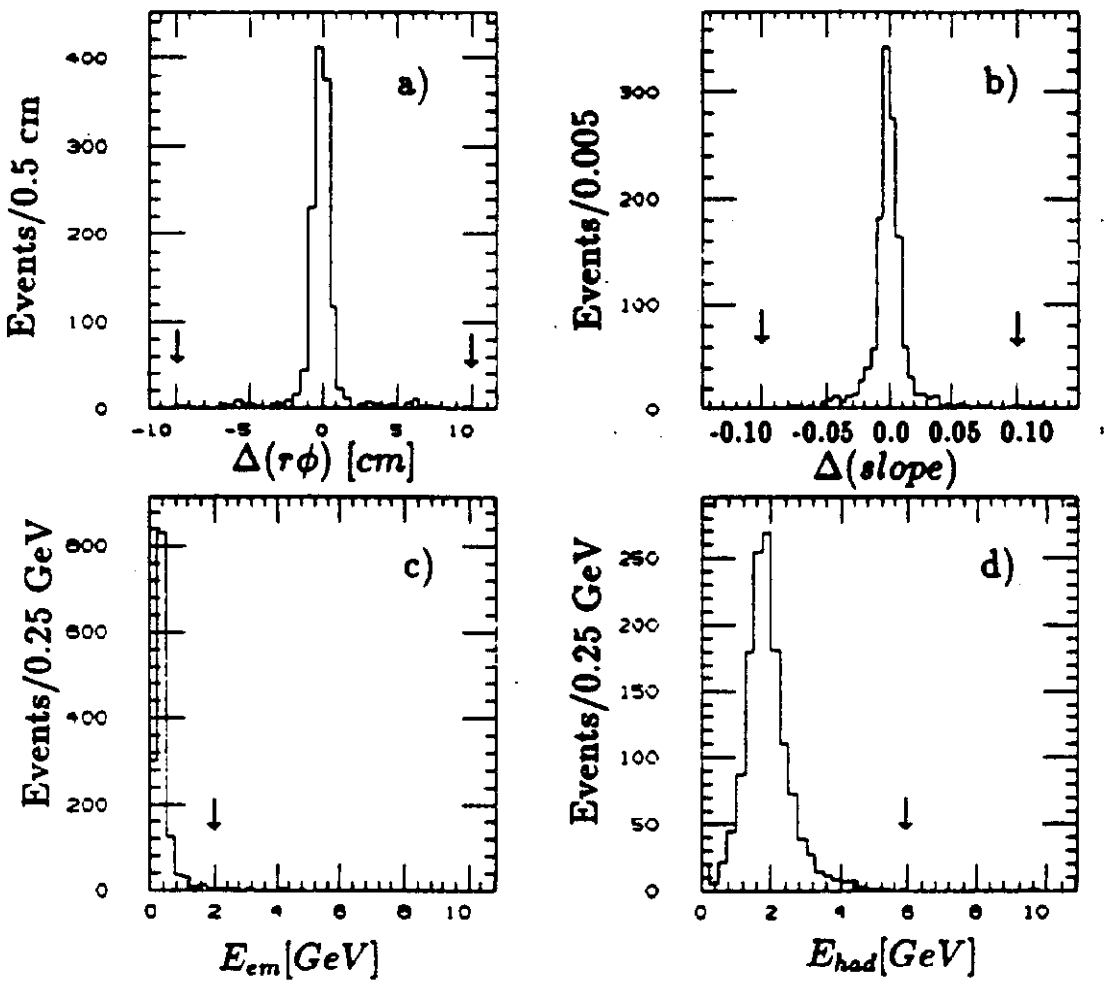

Fig. 6. Distributions of some of the variables used in the CDF muon selection, for a sample of $W \rightarrow \mu\nu$ events obtained with the muon trigger. CTC to muon chamber track matching for a) rϕ position, and b) slope in rϕ. Also, energy deposited by a muon in c) the EM calorimeter and d) the hadronic calorimeter.

cone of $\delta R = \sqrt{\Delta\phi^2 + \Delta\eta^2} = 0.4$ around the muon direction be less than 5 GeV, after the muon energy is subtracted.

For muons inside the fiducial volume and with $P_T > 20$ GeV/c, the efficiencies for the selection criteria were evaluated by using a sample of Z events for which one muon passed the tight cuts. The other muon was used to calculate the efficiencies after cosmic rays and QCD background (no jet with $E_T > 15$ GeV within a δ=0.4 of the muon track) were removed.

Figure 6 shows the distributions of some of the variables used in the muon analysis. These were obtained from a sample of W events satisfying the "muon" trigger, i.e., for which a candidate muon is found in the muon chambers and a loose match with a CTC track was found by the track processor. In the offline analysis a $P_T(\mu) > 20$ GeV/c and a missing E_T >23 GeV (after the muon energy had been included) were required. Similar distributions are obtained from the $Z^0 \rightarrow \mu^+\mu^-$ sample used for the efficiency calculations[16].

6 MONTE CARLO STUDIES

For this analysis we have used the ISAJET[17] Monte Carlo to generate samples of $b\bar{b}$ and $t\bar{t}$ events and the CDF detector simulation program[18] for comparison with the data and the determination of efficiencies.

For $b\bar{b}$ production we have used ISALEP,[19] the special version of ISAJET that efficiently generates bottom pairs produced by higher order diagrams. These include bottom pairs produced by gluon splitting and flavor excitation.

The detector simulation reproduces the data well for most of the cut variables, whereas is slightly off for some others. These differences have been appropriately taken into account in evaluating acceptance and efficiencies.

The Monte Carlo program PAPAGENO[13] has also been used to study the acceptance for top production.

7 CHARACTERISTICS OF THE $e\mu$ EVENTS

Using the electron and muon selection criteria described in Secs.3 and 4, 45 opposite sign $e\mu$ candidate events were found in the 4.4 pb^{-1} of data. Figure 7a shows a scatter plot of $E_T(e)$ vs. $P_T(\mu)$ for these events. The same scatter plots for Monte Carlo generated $t\bar{t}$ and $b\bar{b}$ events are shown for $b\bar{b}$ (.64 pb^{-1}), M_{top} = 28 GeV (2.1 pb^{-1}), and 70 GeV (79 pb^{-1}) in b, c, and d respectively.

Figure 7 shows that the t quark decays produce leptons at larger P_T than the b quarks.

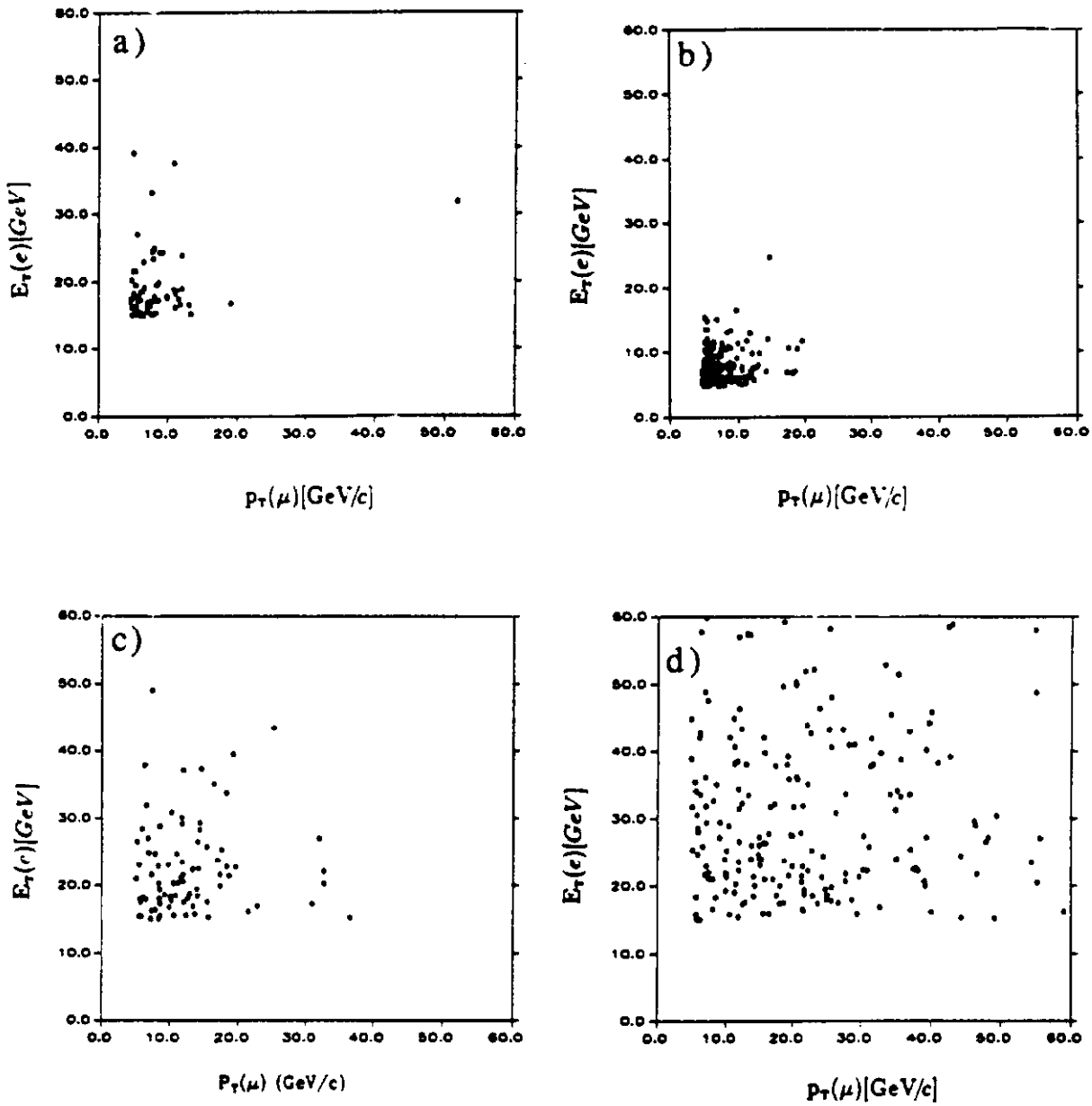

Fig. 7. Scatter plots of the electron E_T versus the muon P_T for a) the data (4.4 pb^{-1}); b) the $b\bar{b}$ Monte Carlo (0.64 pb^{-1}); and top Monte Carlo c) for M_{top}=28 GeV (2.1 pb^{-1}), and d) for M_{top}= 70 GeV (79 pb^{-1}).

This can easily be seen in Fig. 8 which shows the expected number of events in 4.4 pb^{-1} of data with electron $E_T \geq cP_T^{min}$ and muon $P_T \geq P_T^{min}$ as a function of the threshold P_T^{min}, as obtained by the Monte Carlo simulation for $b\bar{b}$ production and the same two top masses.

Figure 9 shows the expected $e\mu$ angular correlation for the data (a) and for the same samples of Monte Carlo events. We plot the minimum of the electron E_T or muon P_T versus the opening angle, $\delta\phi$, of the two leptons. The Monte Carlo shows that for top events the e and the μ tend to be back to back, whereas for the bottom events there is both forward and backward peaking. The data seems most consistent with the $b\bar{b}$ behavior. The $b\bar{b}$ Monte Carlo data was obtained with ISALEP (Sect. 6), for 5 GeV cuts on both the muon P_T and the electron E_T.

We have also analyzed the data obtained with the $e\ \mu$ trigger described earlier. Here both leptons were required to be above a P_T of 5 GeV. Figure 10 shows the opening angle in ϕ between the two leptons for a sample of 1.8 pb^{-1} of data from this trigger. The ϕ angle between same sign and opposite sign leptons is shown in Figs. 10a and 10b, respectively. Figs. 10c and 10d show the same distributions for the bottom Monte Carlo. For opposite sign dileptons, the data and the Monte Carlo show peaking in both the small and large opening angle regions. The enhancement at small opening angle is expected from two separate effects: sequential b→c→ lepton decays and gluon splitting processes for which the b and the $\bar{b}$ have a small opening angle.

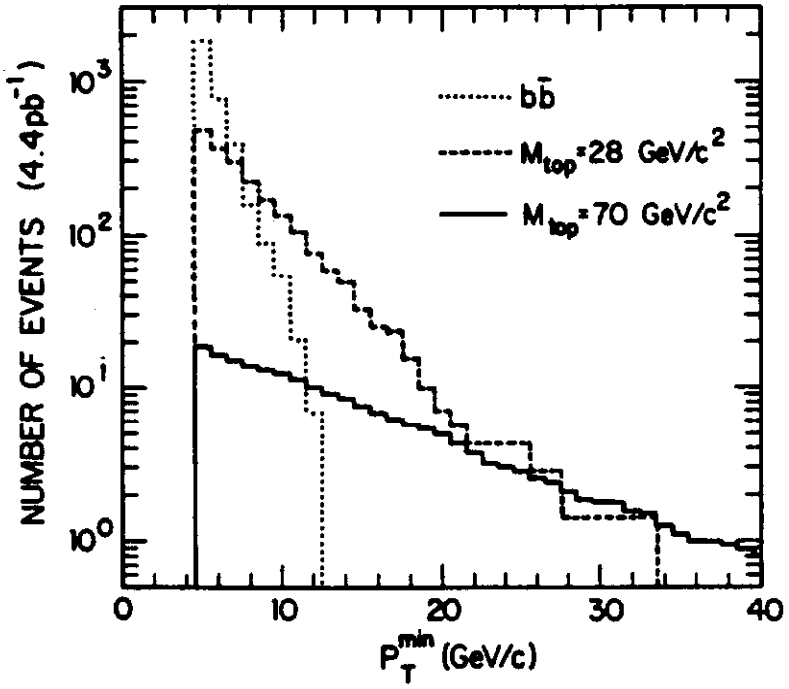

Fig. 8. The expected number of events in 4.4 pb^{-1} in the chosen top signal region as a function of the threshold P_T^{min} for simulated events. Expectations for $t\bar{t}$ production with M_{top}=28 and 70 GeV and for $b\bar{b}$ are shown. The distributions are extended down to 5 GeV/c in this plot in order to see the shape of the $b\bar{b}$ background at low P_T.

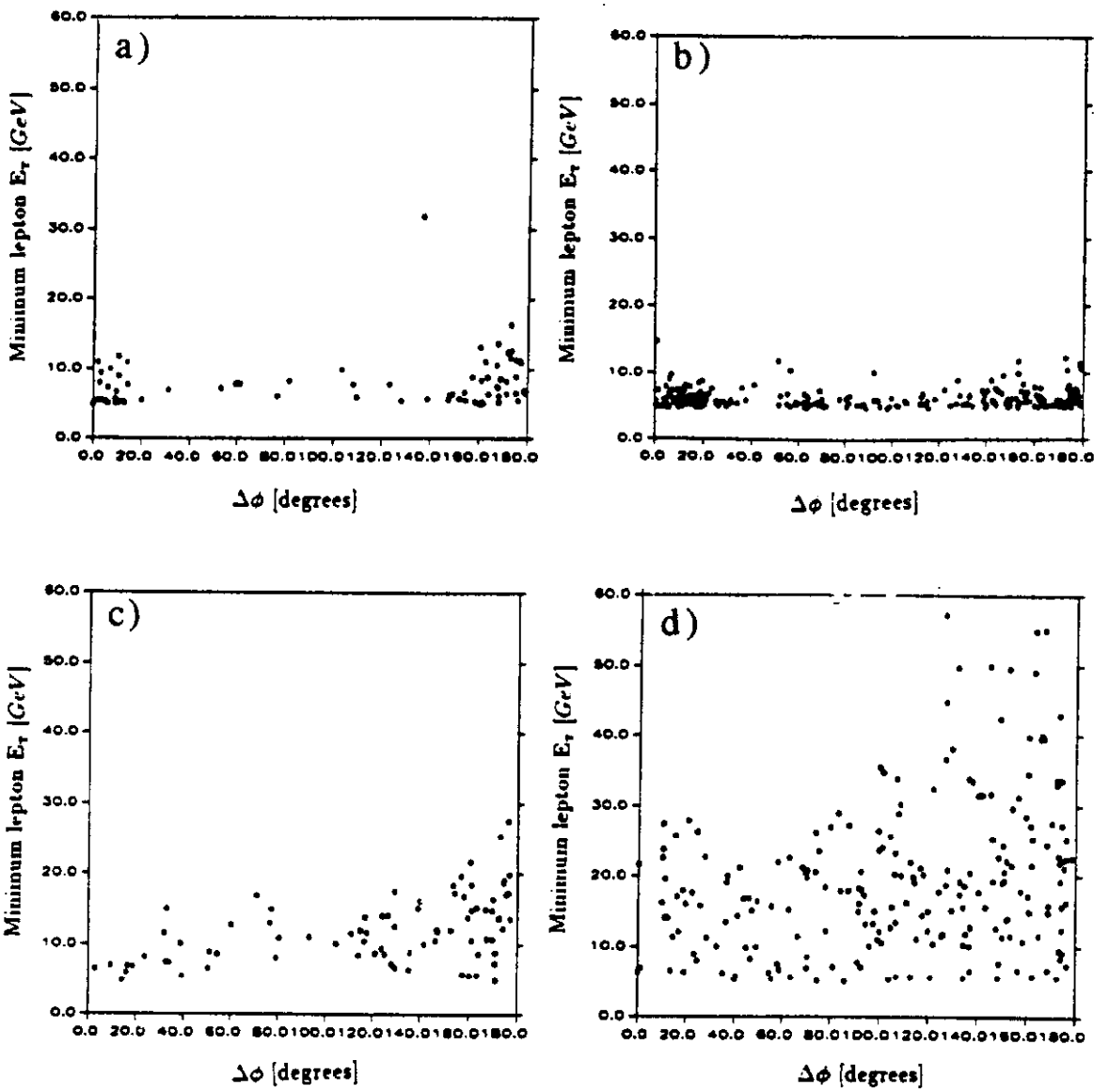

Fig. 9. Scatter plots of the minimum lepton transverse energy vs. the azimuthal $e\mu$ angle difference for the data a) and the same Monte Carlo samples as in Figure 7.

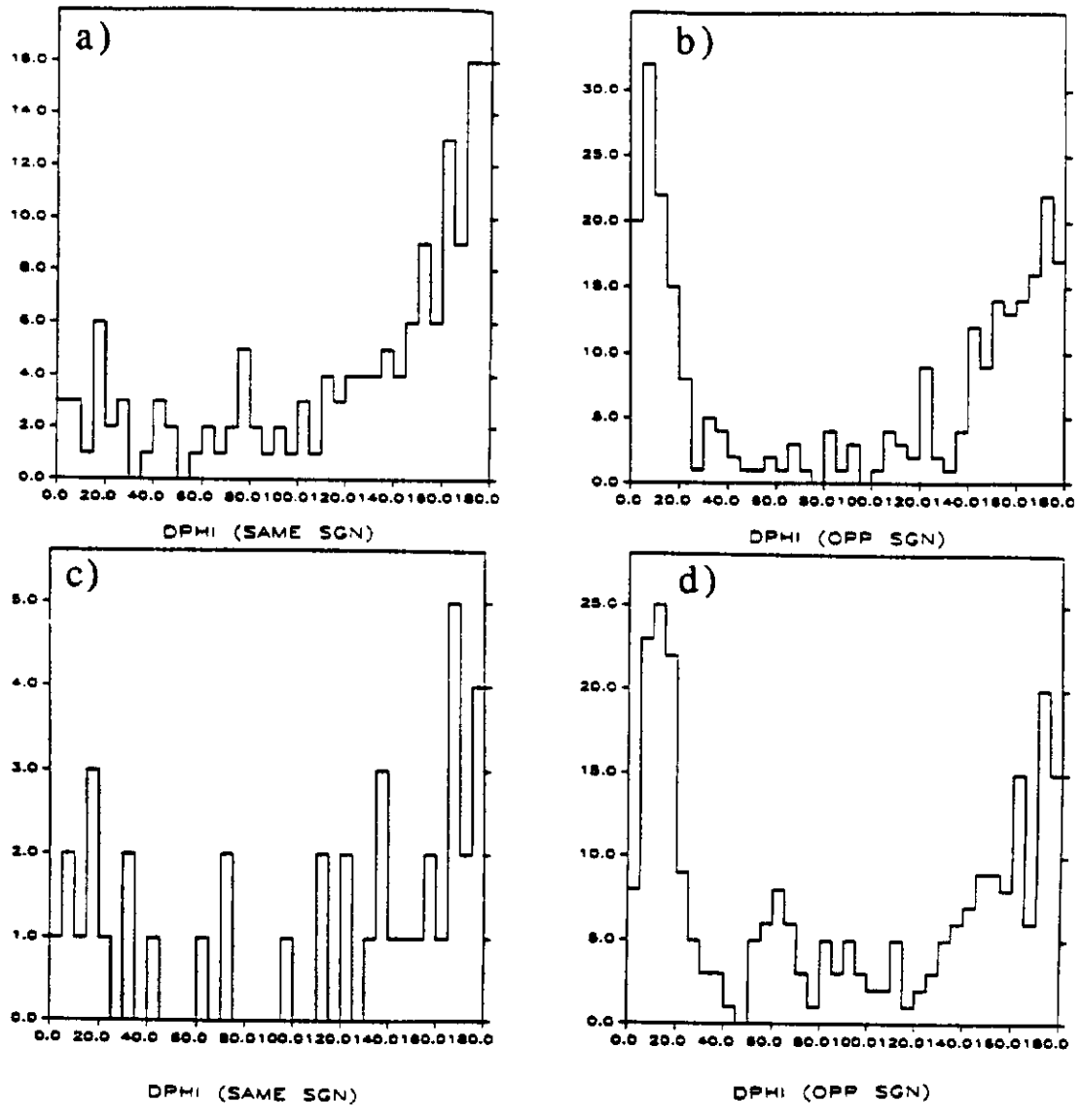

Fig. 10. The azimuthal opening angle for the same sign $e\mu$ samples in a) the $e\mu$ trigger data($1.8pb^{-1}$) and c) the $b\bar{b}$ Monte Carlo, and for the opposite sign $e\mu$ sample in b) the data and d) the $b\bar{b}$ Monte Carlo.

Another variable studied is the isolation of the electron candidates. The energy surrounding the electron candidate in a cone $\delta R = 0.7$ is expected to be different for electrons from top and bottom decays, the latter being less isolated. The isolation variable

$$I = \frac{E_T(\delta R = 0.7) - E_T(e)}{E_T(e)}$$

is shown in Fig. 11 for the 1.8 pb^{-1} of data (a), the $b\bar{b}$ Monte Carlo (b), and the two Monte Carlo top samples (c,d). The data resembles the $b\bar{b}$ Monte Carlo.

The analysis of the data obtained with this trigger is still in progress. The point being made here is that the data has the characteristics expected for bottom production.

The rate of bottom production expected from QCD is uncertain by at least a factor two[20] when next to leading order calculations are used[9,11]. A preliminary study of our data indicates that the observed rate of events is in agreement with these predictions.

We conclude that the data, from both the "inclusive electron" trigger and the $e\ \mu$ trigger are consistent with bottom production.

8 TOP QUARK MASS LIMIT

The data from the "inclusive electron" trigger (Figs.7 and 9), shows only one event with high P_T leptons. To extract an upper limit for top production we will only use this sample. As discussed earlier, the trigger efficiency has been found to be 98% for electrons with P_T $\geq$15 GeV.

In order to reduce possible bottom pair production background (see Figs. 7b and 8), we define the signal region to be:

$$E_T(e) > 15 \text{ GeV} \quad \text{and} \quad P_T(\mu) > 15 \text{ GeV}.$$

The data contain one event in this region. This event (Figure 12) has an isolated electron with $E_T(e)$=31.7 GeV and an isolated opposite sign muon with $P_T(\mu)$=42.5 GeV/c; the dilepton azimuthal opening angle is 137 degrees.

In the signal region, background from $b\bar{b}$ (Fig. 8) and from charged hadrons misidentifed as leptons is not likely to contribute because these signals are not isolated and are concentrated below the lepton thresholds chosen. Backgrounds that could populate the signal region giving $e\mu$ pairs are:

- $Z^0 \rightarrow \tau\bar{\tau}$
- $Z^0 \rightarrow b\bar{b}$

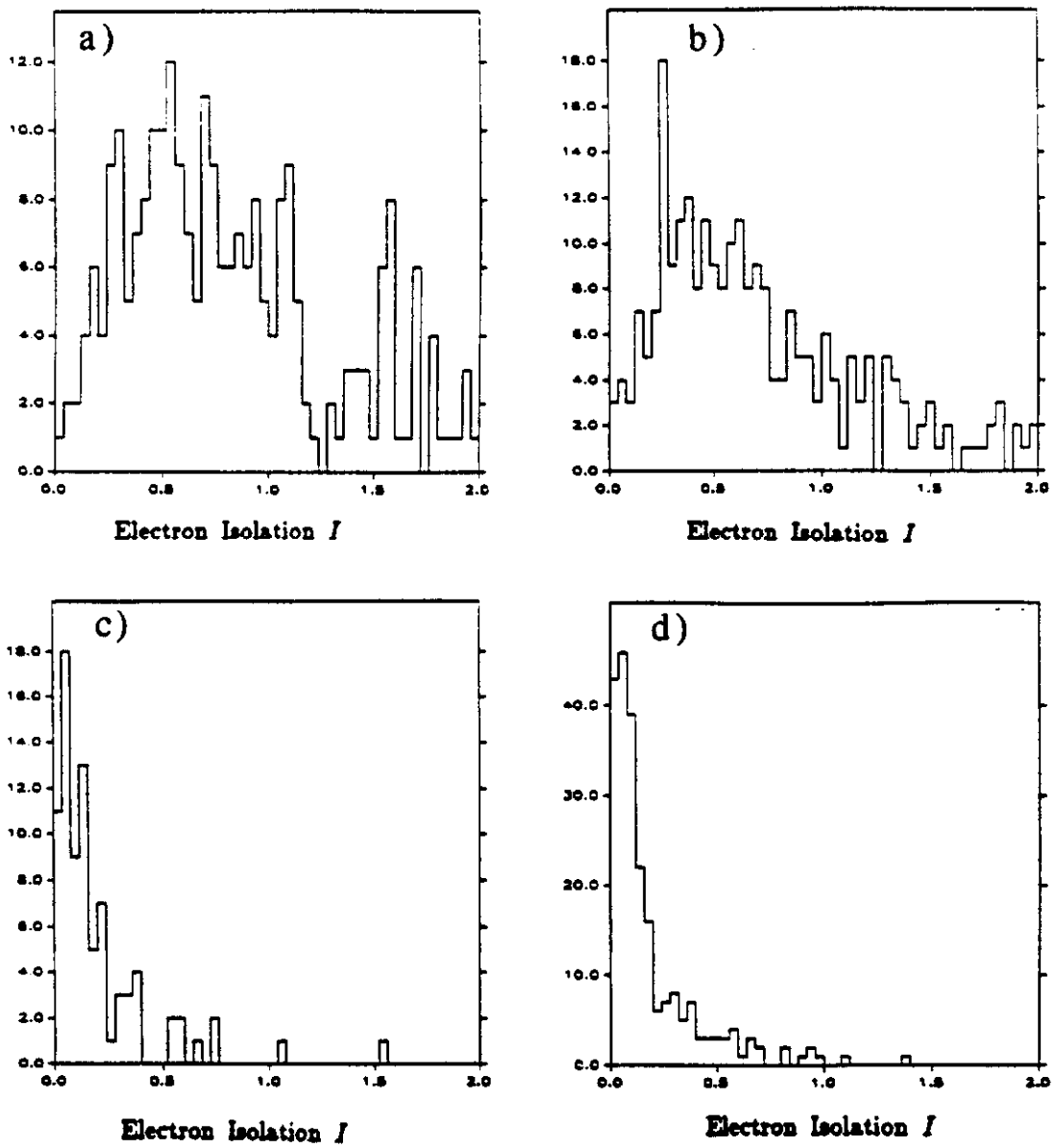

Fig. 11. Distribution of the electron isolation variable I, as defined in the text, for a) the $e\mu$ trigger data($1.8pb^{-1}$), b) the $b\bar{b}$ Monte Carlo; and the $t\bar{t}$ Monte Carlo with c) M_{top}=28 GeV and d) M_{top}= 70 GeV.

- Diboson production, WW and WZ.

In our data sample we expect one event from the process $Z^0 \rightarrow \tau\bar{\tau}$ and 0.2 events from the process $Z^0 \rightarrow b\bar{b}$. The expected number of events for WW production is 0.15 and for WZ is 0.05. For leptons of such high momenta ($E_T(e) > 30$ GeV and $P_T(\mu) > 40$ GeV/c) the probality of $Z^0 \rightarrow \tau\bar{\tau}$ is $\leq 1\%$.

Given the one observed event we can calculate an upper limit for the $t\bar{t}$ production cross section as a function of the top mass. The acceptance and efficiency as a function of the top mass are shown in Fig.13. Separate curves are shown for the various components of the detection efficiency: i) the fraction of the $e\mu$ spectra accepted by the lepton transverse momenta cuts; ii) the geometrical acceptance, which includes the η region accepted for the electron and the muons, as well as the fiducial cuts; iii) the efficiencies for the selection of the $e\mu$ events, Tables I and II, and finally iv) the overall detection efficiency in this analysis (curve labelled total).

The systematic error on the acceptance arising from uncertainties on the transverse energy spectrum of electrons and muons from top decays and on the η distribution have been evaluated by Monte Carlo by comparing results from two Monte Carlos (ISAJET and PAPAGENO). To evaluate the systematic error due to lack of knowledge of the top fragmentation into hadrons, the parameters of the Peterson fragmentation function[21] were varied in both Monte Carlos over a wide range. The uncertainty from these two sources vary from 40% at 28 GeV to 5% at 70 GeV. The uncertainties on the fiducial cuts and on the event selection are 3% each. The uncertainty on the luminosity is 15%. The systematic uncertainties, assumed to be Gaussian, are added in quadrature and then convoluted with a Poisson distribution for the one observed event, to calculate an upper limit for the observed number of events at each top mass.

Finally, using the detection efficiency described above, the luminosity and the upper limit of the events in the signal region, we calculate a 95% confidence level upper limit for the observed $t\bar{t}$ cross sections as a function of the top mass. The expected number of events for top production vary from 33 to 7.5 over the 28 to 72 GeV mass interval. The cross section upper limits are shown in Fig. 14. The cross sections of Fig. 1 with their uncertainties are also shown in the same figure. The CDF upper limit and the lowest expected cross section curve intersect at 72 GeV. Thus these data exclude top production in $p\bar{p}$ collisions at 1.8 TeV in the 28 to 72 GeV mass interval at the 95% confidence level.

The production cross section for a fourth generation quark, b', of charge -1/3, is expected to be the same as for the t quark. Assuming the b' to decay via charged currents into a light quark and a virtual W, these data exclude production of such a quark in the mass range 28 to 72 GeV/c.

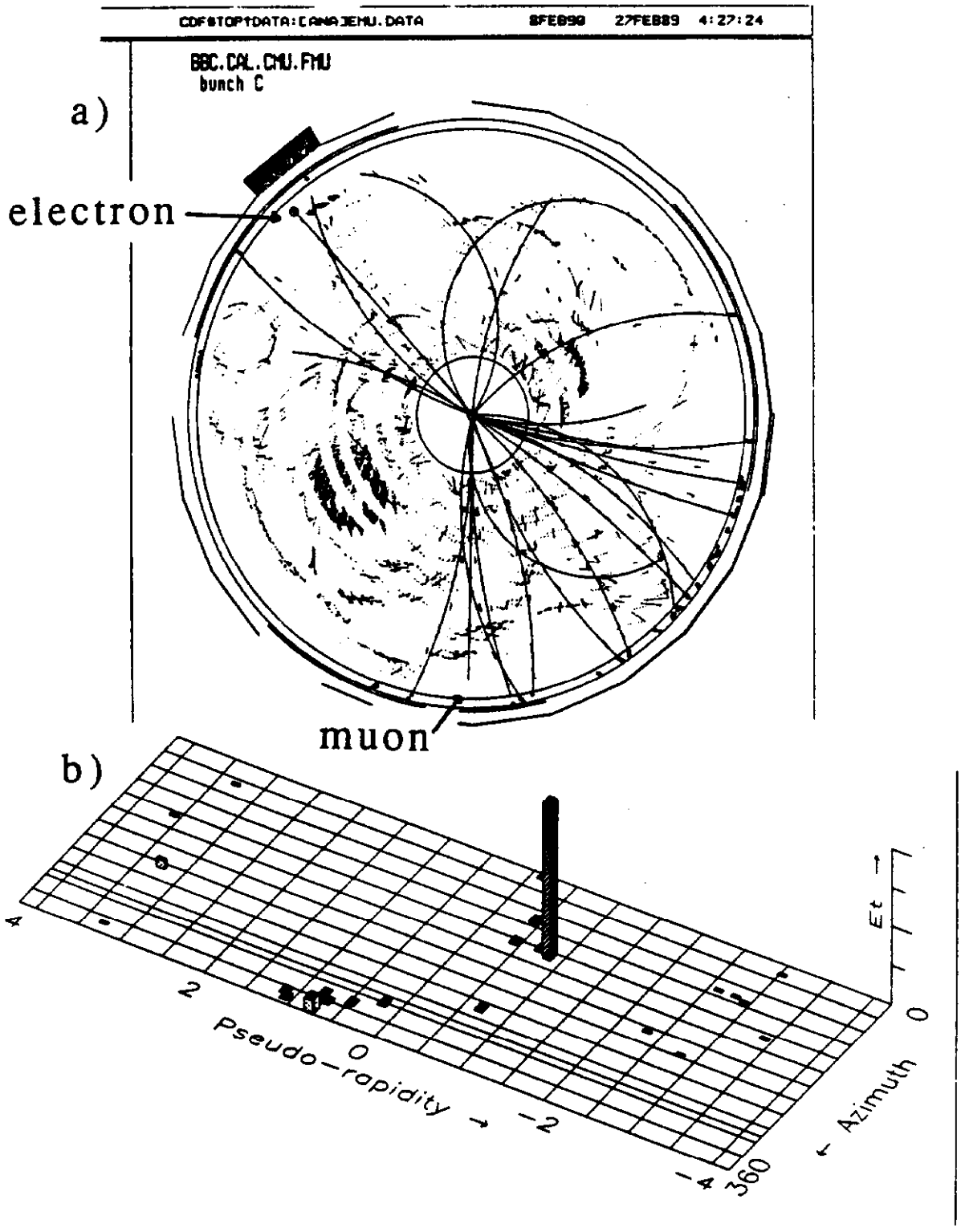

Fig. 12. The one candidate event. a) the $r\phi$ view: the electron at ϕ= 130^0 has E_T=31.7 GeV, the μ at ϕ=260^0 has P_T=42.5 GeV/c. b) the azimuth vs. η plot, with the vertical scale representing the calorimeter energy. The electron is the large tower at ϕ=130^0, the μ is at η=-0.7 and ϕ=260^0.

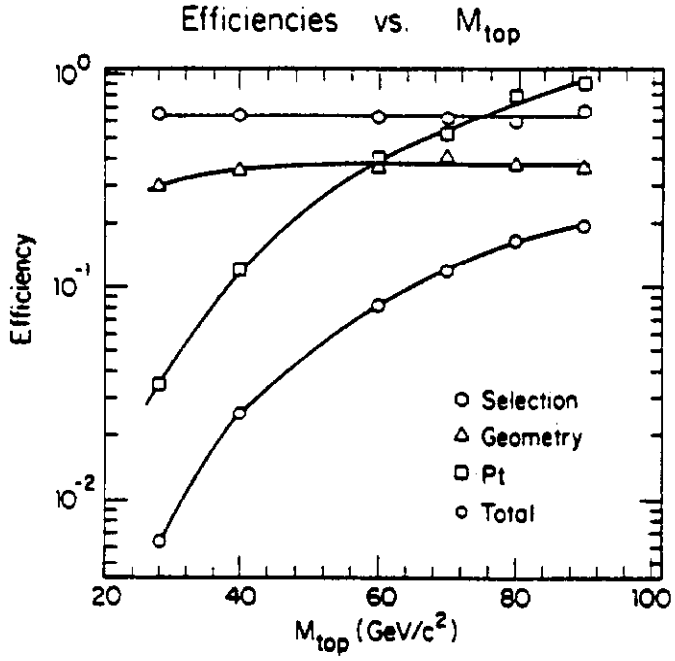

Fig. 13. Detection efficiencies for $e\mu$ pairs from $t\bar{t}$ production, as a function of the top mass, for: i) the P_T requirement; ii) the geometric acceptance (both η and fiducial cuts); iii) the dilepton identification cuts, and iv) total. The branching ratio into $e\mu$ is assumed to be 100% in this plot.

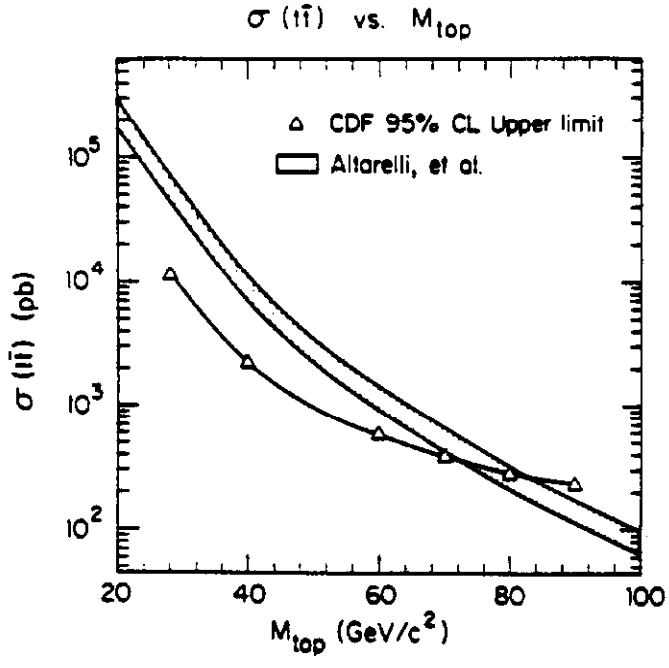

Fig. 14. The 95% confidence level upper limit on the $t\bar{t}$ production cross section as function of the top mass. The shaded bands show the $t\bar{t}$ production cross sections of Fig. 1.

REFERENCES

1. J.E. Augustin et al., Phys. Rev. Lett. 33, 1406 (1974); J.J. Aubert et al., Phys. Rev. Lett. 33, 1404 (1974).

2. S.W. Herb et al., Phys. Rev. Lett. 39, 252 (1977).

3. T. Kamae, Proceedings of the XXIV International Conference on High Energy Physics, Munich (1988), ed. R. Kotthaus and J. Kuhn, Springer-Verlag (1989), p. 156.

4. C. Albajar, et al., Z. Phys. C37, 505 (1988); I.J. Kroll, Proceedings of the XXIV International Conference on High Energy Physics, Munich (1988), ed. R. Kotthaus and J. Kuhn, Springer-Verlag (1989), p. 1416.

5. A. Buras and J.M. Gerard, Phys. Lett. 203B, 272 (1988).

6. U. Amaldi et al., Phys. Rev. D36, 1385 (1987).

7. F. Abe et al. (CDF Collaboration), Nucl. Instrum. Methods A271, 387 (1988).

8. R. K. Ellis, "The theory of heavy flavor production", lectures delivered at the SLAC Summer Institute, July 1989.

9. P. Nason, S. Dawson and R.K. Ellis, Nucl. Phys. B303, 607 (1988).

10. M. Diemoz, F. Ferroni, E. Longo and G. Martinelli, Z. Phys. C39, 21 (1988).

11. G. Altarelli, M. Diemoz, G. Martinelli and P. Nason, Nucl. Phys. B308, 724 (1988).

12. B. Williams, (CDF Collaboration), "Search for the top in $e+$ jets events at CDF", (these Proceedings).

13. I. Hinchliffe, "Application of QCD to Hadron Collider Physics (Theory)", Lectures delivered at the SLAC Summer Institute, July,1989.

14. F. Abe et al., (CDF Collaboration), Phys. Rev. Lett. 63, 720 (1989).

15. J. Proudfoot, "Electron identification in the CDF calorimeter", Note CDF-935, to be published in the Proceedings of the Tascalousa SSC Workshop on Calorimetry for the Supercollider (March, 1989).

16. M. Contreras, "Search for the top quark in electron-muon events at the Tevatron Collider", PHD Thesis, Brandeis University (1990).

17. F. Paige and S.D. Protopopescu, BNL Report No. BNL 38034, (1986) (unpublished).

18. J. Freeman, Proceedings of the Workshop on Detector Simulation for the SSC, ed. L.E. Price, Argonne National Laboratory, p. 190 (1987).

19. The ISALEP version of ISAJET was first developped by UA1. Frank Paige has made it available to us.

20. P. Nason, S. Dawson, R.K. Ellis, preprint FERMILAB-Pub-89/91-T, Nuclear Physics B(in press).

21. C. Peterson, D. Schlatter, I. Schmidt and P. Z. Zervas, Phys. Rev. D27,105(1983).